energies

MDPI

Review

Directions of Development of Diagnostic Methods of Vacuum Medium-Voltage Switchgear

Paweł Węgierek *, Damian Kostyła and Michał Lech

Faculty of Electrical Engineering and Computer Science, Lublin University of Technology, Nadbystrzycka 38 A, 20-618 Lublin, Poland
* Correspondence: p.wegierek@pollub.pl; Tel.: +48-81-538-43-47

Abstract: The development of power grid infrastructure and increasingly stringent environmental regulations have intensified work, carried out by researchers and electrical equipment manufacturers, to develop innovative gas-insulated, environmentally neutral devices. The emergence of new designs of circuit breakers and disconnectors, in which the resulting electric arc is extinguished in a vacuum environment, requires the development of appropriate techniques for diagnosing the chambers responsible for the dielectric parameters of the device. The following article presents an overview of the directions of development of diagnostic methods for medium-voltage vacuum switching equipment, which can potentially be used to develop a real-time pressure monitoring system that can be applied to vacuum switching equipment used in electrical infrastructure.

Keywords: vacuum technology; vacuum degree; pressure level; vacuum condition; vacuum measurement; dielectric strength; real-time monitoring; vacuum interrupter

check for updates

Citation: Węgierek, P.; Kostyła, D.; Lech, M. Directions of Development of Diagnostic Methods of Vacuum Medium-Voltage Switchgear. *Energies* **2023**, *16*, 2087. https://doi.org/10.3390/en16052087

Academic Editor: Xiao-Hua Wang

Received: 30 December 2022
Revised: 10 February 2023
Accepted: 16 February 2023
Published: 21 February 2023

Copyright: © 2023 by the authors. Licensee MDPI, Basel, Switzerland. This article is an open access article distributed under the terms and conditions of the Creative Commons Attribution (CC BY) license (https://creativecommons.org/licenses/by/4.0/).

1. Introduction

Electricity is one of the basic utilities used in today's world. It is essential in almost every area of our lives, from powering large manufacturing plants to protecting human health and life. The ever-increasing amount of electricity consumed by consumers and the increased demands placed on networks in terms of continuity and quality of energy supply have led to the development of energy infrastructures [1–3], which is constantly being improved to meet the challenges posed. Innovative technologies are being applied to modern networks and have prompted the development of appropriate control and measurement techniques to verify the condition of the power network in operation [4]. The development of the electricity network has led to an increase in the importance of gas-insulated apparatus, particularly the importance of vacuum interrupter technology (VI—Vacuum Interrupters), whose main aspect of suitability for operation is the pressure inside the extinguishing chamber. Given the paramount importance of the pressure level in a vacuum chamber, the power industry faced another challenge of developing a real-time pressure measurement system to enable chamber diagnostics and thus predict potential damage and thus power outages. To the best knowledge of the article's authors, there is currently no technology solution for continuous pressure measurement designed for equipment operating in continuous mode. In connection with the work carried out, by the research group, on the development of the aforementioned system for monitoring the parameters of a vacuum chamber in on-line mode, the state of the art of selected methods of measuring pressure in vacuum equipment was analyzed and compared, which could potentially be used to develop a system for monitoring the pressure of vacuum quench chambers in real time.

2. Switching Devices in Medium-Voltage Networks

The VI technology, especially modern vacuum circuit breakers (VCBs—Vacuum Circuit Breakers) are of enormous importance in the power system, enabling switching processes

to be carried out autonomously or with negligible dispatcher intervention. Vacuum circuit breaker technology is widely known and used in network infrastructure, mainly through the VD 4 series from ABB [5] and the SION series from SIEMENS [6]. Vacuum circuit-breakers practically dominate the switchgear in transformer substations due to their small size and excellent mechanical durability of up to 30,000 switching cycles, as well as the fact that no maintenance is required during normal operation.

Over the decades, the market for arc extinguishing agents has been dominated by vacuum, this was not always the case, as shown in Figure 1 below.

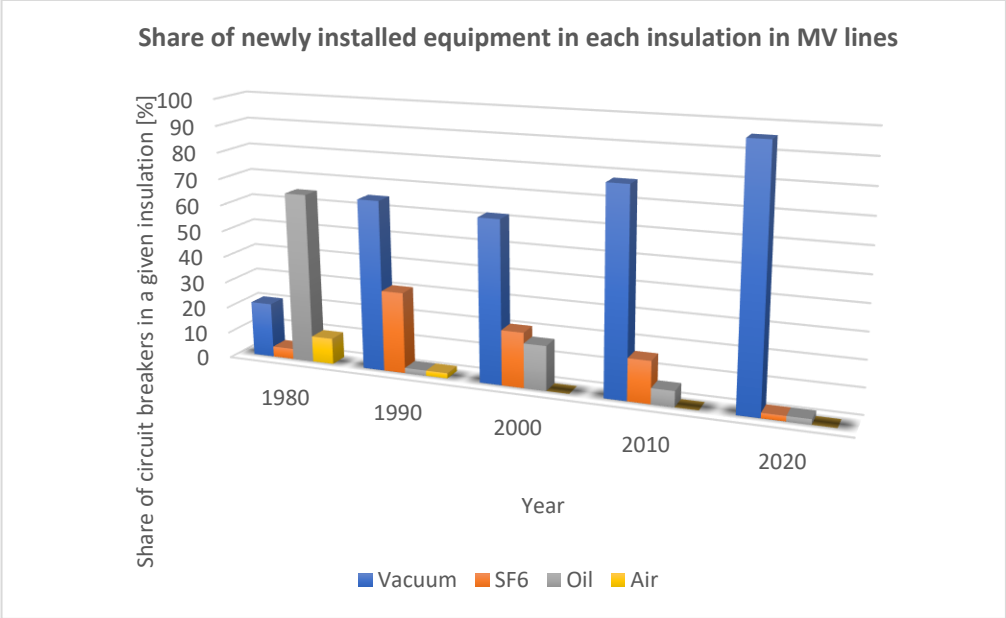


Figure 1. Proportion of each type of equipment in the total number of installed apparatuses [7].

As can be seen from the diagram above, oil, air, sulfur hexafluoride (SF_6) and vacuum have played the role of insulating medium in switchgear over more than four decades [8].

In the 1980s, oil-insulated circuit breakers were the most trusted. The entire circuit breaker unit was immersed in a tank filled with oil, whose function was to provide insulation and an arc extinguishing mechanism. These were usually located outside [9]. However, the great days of oil-insulated circuit breakers are already long gone and now they have been virtually eliminated from industrial applications in favour of vacuum circuit breakers.

Pneumatic air circuit breakers [10–12] have been used extensively in various types of circuits, especially conditions. They are equipped with blast coils, applicable for arc extinguishing by magnetic blast, and blast tubes that operate by forcing air down the tube from each nozzle of the contact assembly. They were completely displaced from the market in favour of vacuum units more than two decades ago.

Another type of gas-insulated apparatus encountered in networks are arc extinguishing switches in compressed SF_6 [13,14]. In industrial environments where the use of oil circuit breakers was not possible due to fire hazards. The cool air created by convection enables them to operate at the correct temperature for the operating.

Sulfur hexafluoride and vacuum circuit breakers are similar in design. The main difference between these two apparatuses is the insulation, which is provided by different dielectric medium. The highly compressed gas is expelled from the arcs in the circuit breakers while the mechanism is operating and is then collected in a low-pressure container before being transported back to the high-pressure container for reuse. The effect of extinguishing the arc in SF_6 is an extremely harmful residue from arc combustion. The fact that SF_6 is a powerful greenhouse gas is also not insignificant. The pollutants released into the environment can have a very negative impact on the atmosphere. The technology used reduces the possibility of leakage from the circuit breaker during operation.

The most common adaptation of circuit breakers for more than four decades has been vacuum circuit-breakers [15,16]. This solution is nowadays widely used in various types of power systems. They are famous for their long service life and functionality and, above all, for their lack of negative environmental impact, which is extremely important in the context of an ongoing environmental policy. They provide a higher degree of reliability compared to air circuit breakers. Due to the fact that there is no ionizing agent and only the contact material is present, vacuum circuit breakers are characterized by low arc energy. The arc is extinguished already at a distance between contacts of 2–3 mm (typically 10 mm for MV networks). Near the point where the current passes zero, the discharge can no longer be maintained by the arc energy and the arc is extinguished.

As Figure 1 shows, for almost forty years there has been a constant increase in the amount of equipment in which vacuum technology is used, which has been reflected in the work of scientists and in the innovative designs of vacuum-insulated apparatus offered by manufacturers. in the work of researchers and in the innovative designs of vacuum-insulated apparatus offered by manufacturers. The dynamic development of the grid and stricter regulations on power outages have necessitated the development of new designs of vacuum equipment.

In countries with a low level of network cabling, such as Poland, medium-voltage overhead networks play a decisive role in shaping reliability factors. Inherent in these networks are disconnectors, which are typically installed in overhead lines, are responsible for connecting operating currents and are most often of open, less often of closed construction, but based on SF_6 technology. It is only in the last decade that research work has been undertaken to develop a vacuum disconnector with a closed design, free of SF_6, using vacuum technology.

The result of the work of researchers and manufacturers of switchgear intended for medium-voltage networks is EKTOS—an innovative medium-voltage overhead vacuum disconnector in a closed enclosure, dedicated to Smart Grids, which was developed in cooperation with researchers from Lublin University of Technology and a company EKTO from Białystok. The innovativeness of EKTOS lies primarily in the innovative, developed from scratch motor storage drive integrated with the contact system which is based on a DC motor, which has allowed the system's dimensions and power requirements to be reduced to 90W. The place of contactors and limit switches has been taken by a starting system equipped with reed switches. In order to eliminate tie rods and thus simplify the design, the entire drive unit was located inside the disconnector structure. This form of drive system, to the authors' knowledge, is not found in other devices of this type [17]. Bearing in mind that EKTOS is a device intended for use on overhead lines, its weight is not without significance. Components with reduced weight and size were used in the construction of the apparatus, which has resulted in the final weight of the device being approximately 1⁄5 that of known construction solutions. It is perfectly in line with global preferences in terms of the direction of network infrastructure development. It has based the operation on an emission-free medium such as vacuum, but there are still improvements in the dielectric resistance of the extinguishing medium through the use of noble gases or mixtures of these gases as an arc-extinguishing medium [18]. Another challenge faced by EKTOS is the need to provide real-time measurement of the gas pressure in the vacuum chamber so that potential damage resulting from unsealing of the extinguishing chambers can be predicted.

2.1. Gas-Insulated Switchgear

The constantly increasing participation of clean, low-carbon, renewable energy sources are extremely important in terms of reducing the amount of greenhouse gases that are supplied to the atmosphere. Currently, the most common switching devices used in electrical networks are circuit breakers, the huge majority of which operate based on gas insulation [19]. These are mainly disconnectors based on sulphurhexafluoride (SF_6) or the vacuum. The necessity to reduce the supply of greenhouse gases to the atmosphere, among others used in electrical appliances, was identified through the Kyoto agreement [20],

or during the 2015 Paris climate conference [21]. The Kyoto Protocol identified SF_6 gas as one of the most potent greenhouse gases, with a global warming potential (GWP) of 22,800 times that of what is referred to as harmful, carbon dioxide (CO_2) [22–24]. Despite this, SF_6 is still widely used on a large scale in grid infrastructure, as an insulating medium in arc extinguishing apparatus, but the latest European Parliament regulation of 5 April 2022 [25] mandating that newly installed or replaced medium-voltage switchgear up to 24 kV, and up to 52 kV being placed on the market after 1 January 2026 and 1 January 2030, respectively, base their insulation on media having a greenhouse potential (GWP_{100}) of no more than 10. The regulation also applies to high-voltage equipment operating at 52 kV to 145 kV and above 145 kV. Appliances placed on the market after 1 January 2028 and after 1 January 2031 may not have an insulating medium with a GWP_{100} above 10. The enactment of this regulation can be considered as the end date for appliances with hexafluoride sulphur insulation. Many studies have been carried out to identify an alternative insulating medium that would successfully replace sulphur hexafluoride. Table 1 shows the greenhouse potential and atmospheric lifetimes of selected gases that have been the subject of these studies.

Table 1. Summary of alternatives to SF_6 gas [26–32].

No.	Gas	Global Warming Potential (GWP_{100})	Atmospheric Lifetime/(Years)
1	Vacuum	0	-
2	CO_2	1	200
3	CF_3I	5	0.05
4	CH_4	27	12
5	$C_2H_4F_2$	140	1.5
6	N_2O	310	120
7	CF_4	6500	50,000
8	NF_2	8000	50–740
9	C_4F_{10}	8700	2600
10	C_4F_8	8700	10,300
11	C_3F_8	8830	2600
12	CHF_3	11,700	390
13	C_2F_6	12,200	10,000
14	SF_6	22,800	3200
15	CO_2	0	-

Finding an environmentally friendly gaseous medium with insulating and quenching properties not inferior to those of sulphur hexafluoride, while being economically affordable other than vacuum, has proven to be a challenge [33]. Vacuum does not allow for the conduction of current in the steady state of the insulation or in the transient state during the shorting or opening of the operating contacts [34]. The change in dielectric properties in vacuum chambers is closely related to the shape and material of the contacts used, the distance between contacts, but it is the pressure inside the apparatus [35] that determines the suitability of the apparatus for operation. VI technology fits well with the prevailing trend towards miniaturization of devices, due to the low volume of the quenching medium, high dielectric resistance for small inter-contact gaps and the lack of maintenance during operation. In addition to a number of advantages, vacuum devices have a number of significant disadvantages, the most significant of which is the lack of an industrially suitable method for real-time monitoring of the pressure inside the device [36] and the generation of switching overvoltage caused by current shear before passing through zero. A comparison of the most significant advantages and disadvantages of vacuum-based and sulphur hexafluoride-based devices is included in Table 2.

Table 2. Overview of the properties of vacuum-insulated and SF_6-insulated equipment [7,19,35,37].

Vacuum Technology (Advantages)	**SF_6 Technology (Disadvantages)**
No need for conservation work during the operating period	The need for frequent maintenance work during the operating period
No influence of outside temperature	Vulnerable to external temperature
No risk of explosion	Risk of explosion at high current levels
No negative impact on the environment	Greenhouse gas with extremely unfavorable decomposition products, specialized disposal equipment required
High breakdown voltage for small contact gaps with large deviations	Lower breakdown voltage for analogous contact breaks but with smaller deviations
The contact system is arc resistant	Requirement for special designs to increase contact life
Low drive energy required for operating mechanism—smaller opening and closing travel	Significant drive energy required for operating mechanism—greater opening and closing travel
Seamless transition to steep transient voltage increase	Problems when switching on/off rapid rise in transient voltage
Opening and closing times with slight deviation—easy controlled disconnection of fault and load currents	Opening and closing times with large deviations—complicated control of disconnection of capacitive and inductive currents
Ability to interrupt large fault currents regardless of the position of the moving contact	Lack of ability to interrupt large fault currents when the moving contact approaches the open position
Arc duration of 5–7 ms	Arc duration of 10–15 ms
Vacuum Technology (Disadvantages)	**SF_6 Technology (Advantages)**
Difficulties in carrying out switching operations for rated currents above 3150 A	Seamless implementation of switching operations for rated currents above 3150 A
No real-time monitoring of pressure status during operation	Easy real-time monitoring of quality and pressure during operation
X-ray emission of 5.0 µSv·h-1 under normal operating conditions	No X-ray emission under normal operating conditions
High number of arc re-ignitions when combining inductive currents due to high frequency current interrupting capability	Low number of re-ignitions when combining inductive currents
Generating switching overvoltage's due to current clipping before natural zero crossing	No switching overvoltage generation

Higher switching capacity and short contact changeover operation times are essential for vacuum disconnectors (VCBs) to improve the efficiency of today's power systems. Therefore, many studies have been undertaken to optimize the performance of vacuum disconnectors. Progress in the mechanism that transfers energy to the mechanical drive train to move the contacts in the VCB has resulted in a significant reduction in contact opening (current disconnection) time, which has dropped from eight to five cycles of power frequency current, and now averages three cycles [38–41]. Over the past four decades, many different types of tripping mechanisms have been developed for drive systems, including those based on pneumatic, spring, permanent magnet, digitally controlled motor,

electromagnetic repulsion and other principles [42–44]. The vacuum method can be used to create a fast current circuit-breaker that is controlled by the AC short-circuit current in a short time and realized by a fast vacuum circuit breaker (FVCB—Fast Vacuum Circuit Breaker), also known as fast vacuum breaker technology, which can reduce the breaker time to half a cycle of the short-circuit current [38–45]. The reliable arrangement of the drive mechanism significantly reduces the time of the contact closing and opening operations, which means that the fault condition in which the arc burns is reduced to a minimum.

Although the drive mechanism is of great importance in the quality of the operation of vacuum apparatuses, the vacuum quench chambers are the basic element of these devices.

Vacuum Chambers

A fundamental component of vacuum insulated switchgear are vacuum extinguishing chambers. They are responsible for providing a safe insulation gap in the contact space. The current path is located inside the ceramic or glass enclosure from which the chamber is made. For minimizing contact pad wear during switching operations, the material and shape of the contacts are selected already during the design phase. The use of a resilient bellows, which guarantees the tightness of the system, makes it possible for one of the contacts to move. The chamber contains a condensation screen on which conductive particles are deposited from arcing discharges occurring between contacts. This element is required because conductive particles that have settled on the chamber housing can weaken the dielectric. Vacuum chambers are made with advanced technology which requires the use of unique materials that can withstand pressure differences and mechanical shocks. The pressure inside the extinguishing chamber is typically 10^{-4} Pa [46]. Figure 2 shows a cross-sectional view a sample extinguishing chamber [47,48], while Figure 3 shows selected models of vacuum chambers made by the Tele and Radio Research Network's Łukasiewicz Institute.

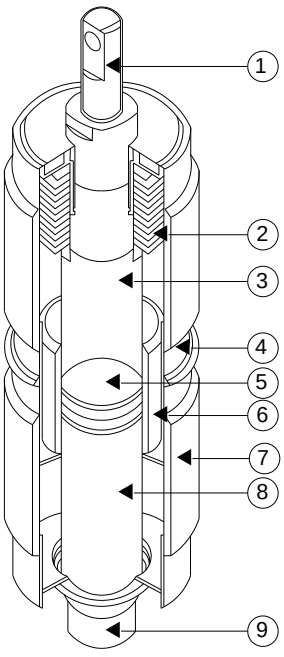


Figure 2. Cross-section of an example vacuum chamber: 1—place of connection to the movable contact, 2—spring bellows, 3—moving pole, 4—ceramic part of the housing, 5—WCu contact, 6—condensation screen, 7—glass part of housing, 8—stationary pole, 9—place of connection to stationary contact.

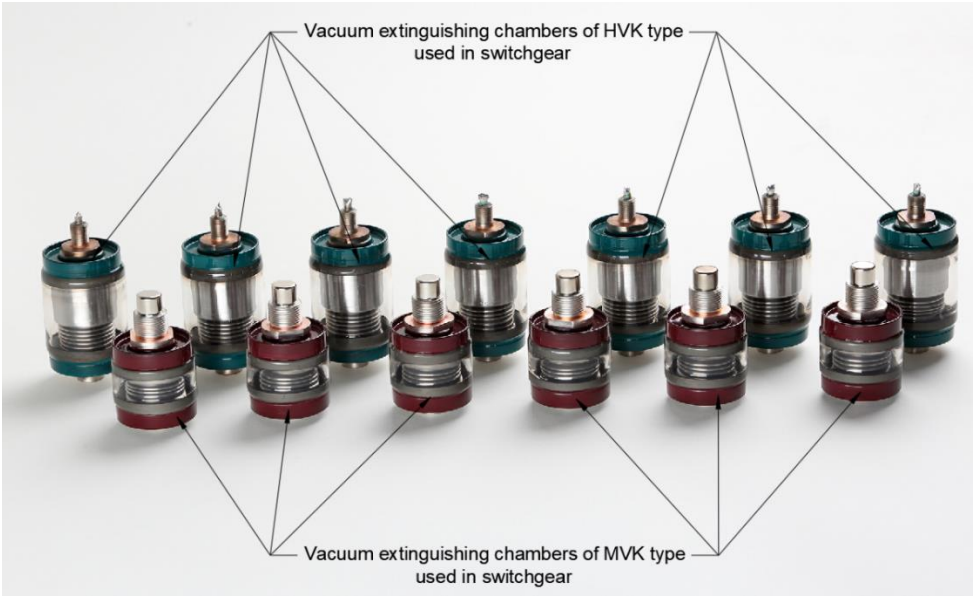


Figure 3. Vacuum chambers used in switchgear [49].

The development of vacuum apparatus technology, as well as the research carried out, has not overlooked one of the most important aspects of development work on vacuum technology—the aspect of pressure control in vacuum chambers.

3. Pressure Control in Switchgear

The control of the pressure level in gas-insulated apparatus is extremely important, as the vacuum retains its excellent insulating properties only up to a pressure level of 1 Pa, once the pressure increases beyond this value the breakdown voltage of the insulating gap drops dramatically [50–52]. This situation is shown in Figure 4 [18,53].

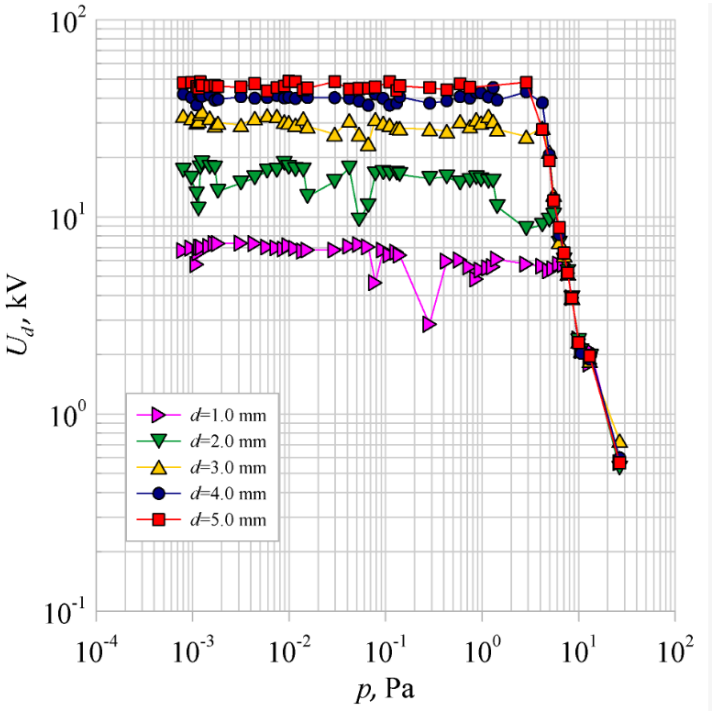


Figure 4. Dielectric strength of the vacuum chamber for different contact distances [18,53].

This is an extremely unfavorable situation, particularly given that the current switchgear used in the power industry is of enclosed construction, which makes it less susceptible to environmental factors and vandalism, but this is coupled with the inability to observe a safe insulation gap. The inability to determine what state the device is currently in poses a number of dangers, the greatest of which is the possibility of potential being transferred to the side that may be de-energized. This poses a serious risk to human health and even life, as maintenance crews carrying out maintenance work on a theoretically de-energized line can be electrocuted. This illustrates the magnitude of the problem of pressure control on gas-insulated equipment. The dielectric strength of the vacuum for different contact distances is shown in Figure 4 [18,53].

The problem of measuring the pressure in vacuum chambers and thus determining the technical condition of these apparatuses affects all equipment that uses vacuum as an extinguishing medium, but it is particularly acute for disconnectors which, due to the specific nature of the switching operations carried out, require knowledge of the pressure prevailing in the extinguishing chamber and thus the ability to determine the presence of a safe insulation gap.

3.1. Chosen Diagnostic Methods for Vacuum Equipment [54]

In answer to a commercial need arising from the lack of a method to detect the degree of vacuum in a device, methods have been developed to determine the serviceability of the device. A summary of the selected methods is shown in Table 3.

Table 3. Diagnostic methods for vacuum equipment [54].

Method	Detection Range [Pa]	Pressure Indication	Operational Applicability
Pening method	10^{-5}–10^{-2}	+	–
the Magnetron method	10^{-5}–10^{-2}	+	–
50 Hz ignition voltages	>1	+	+/–
DC ignition voltages	>1	+	+
AC bonding capacity	$>10^{-2}$	–	+/–
Emission currents	$>10^{-1}$	–	+/–
Emission currents + HF current	10^{-5}–1	+	+
X-ray	$>10^{-1}$	–	+
DC arc voltage	10^{-5}–1	+	+
V_D/V_E	10^{-3}–1	+	+
Screen potential	$10^{-3} + 10^{-1}$	+	–
Induction current switch-off	>0.3	+	+

Most of the presented methods have only found application in laboratory conditions. However, the Pening and Magnetron methods have found favour with vacuum chamber manufacturers as the primary methods for product quality control. The DC static ignition voltage method, on the other hand, is widely used in commercially available vacuum chamber testers. The great potential of the X-ray method has unfortunately been severely limited due to its significant measurement error.

3.1.1. The Pening and Magnetron methods

The main methods that are now being used by vacuum chamber manufacturers are the Pening and Magnetron methods [55]. The principle of their operation consists in subjecting the chamber to a strong axial magnetic field, followed by the application of a DC voltage of the value of 10–20 kV to the open contact system. Under the application of this voltage, an electron emission phenomenon occurs, which, combined with the influence of the axial magnetic field, forces the electrons to spiral towards the cathode, making the path between the contacts much longer, and thus causing many more collisions with particles of the residual gas. The resulting collisional ionization is reflected in the measured current, the value of which enables the magnitude of the prevailing pressure in the chamber to be

determined. For the measurements to be possible, it is necessary to first determine, for each design of apparatus under test, the characteristics of the current-pressure relationship. Moreover, due to the necessity of placing the test object in a strong magnetic field, they are only used in laboratory measurements [56].

3.1.2. DC Static Voltage Ignition Method

Producers of test and diagnostic equipment for vacuum devices consider the static DC ignition voltage method to be the best method for determining instrument pressure [36]. This method involves applying a voltage of a certain value to the device and measuring a current, the value of which should not exceed 30 mA. From this, it can only be determined whether the device is operational or not. Unfortunately, the static DC ignition voltage method can be skewed by conditioning discharges, and the measurement accuracy itself is also unsatisfactory [54]. A device using this method is the Vidar vacuum chamber tester presented in Figure 5.



Figure 5. Vacuum chamber tester Vidar [57].

3.1.3. X-ray Measurement Method

The negative fact of X-ray emission has found a positive application in the method of pressure determination. The method is based on the fact that the intensity of the radiation is directly proportional to the emission currents generated, and its undoubted advantage is the possibility of non-contact measurement and the lack of need to change the position of the contacts or interfere with the operation of the apparatus. An impediment to the widespread use of this method is the radiation interference caused by natural terrestrial radiation, which in the case of tests of such small values results in significant measurement distortions [33,54,58].

3.2. Determination of Pressure Status in Real Time

The methods shown in Figure 5, even though capable of determining the pressure during the operation of the device, do not allow real-time measurements to be made. A measurement taken at any time does not guarantee correct operation in the future. In addition, depending on the method used for inspection, it may be required to take a section of the line out of service in order to remove the apparatus and transport it to the laboratory for voltage testing and to shut down the line again in the event of a fault, thereby increasing reliability factors. A major concern is the safety of the crews working on the

line, as a chamber tested by traditional methods does not guarantee correct operation in the near term. Typical methods used in industry to determine pressure levels in vacuum chambers, together with a breakdown of the pressure ranges for which they can be used, are summarized in Figure 6.

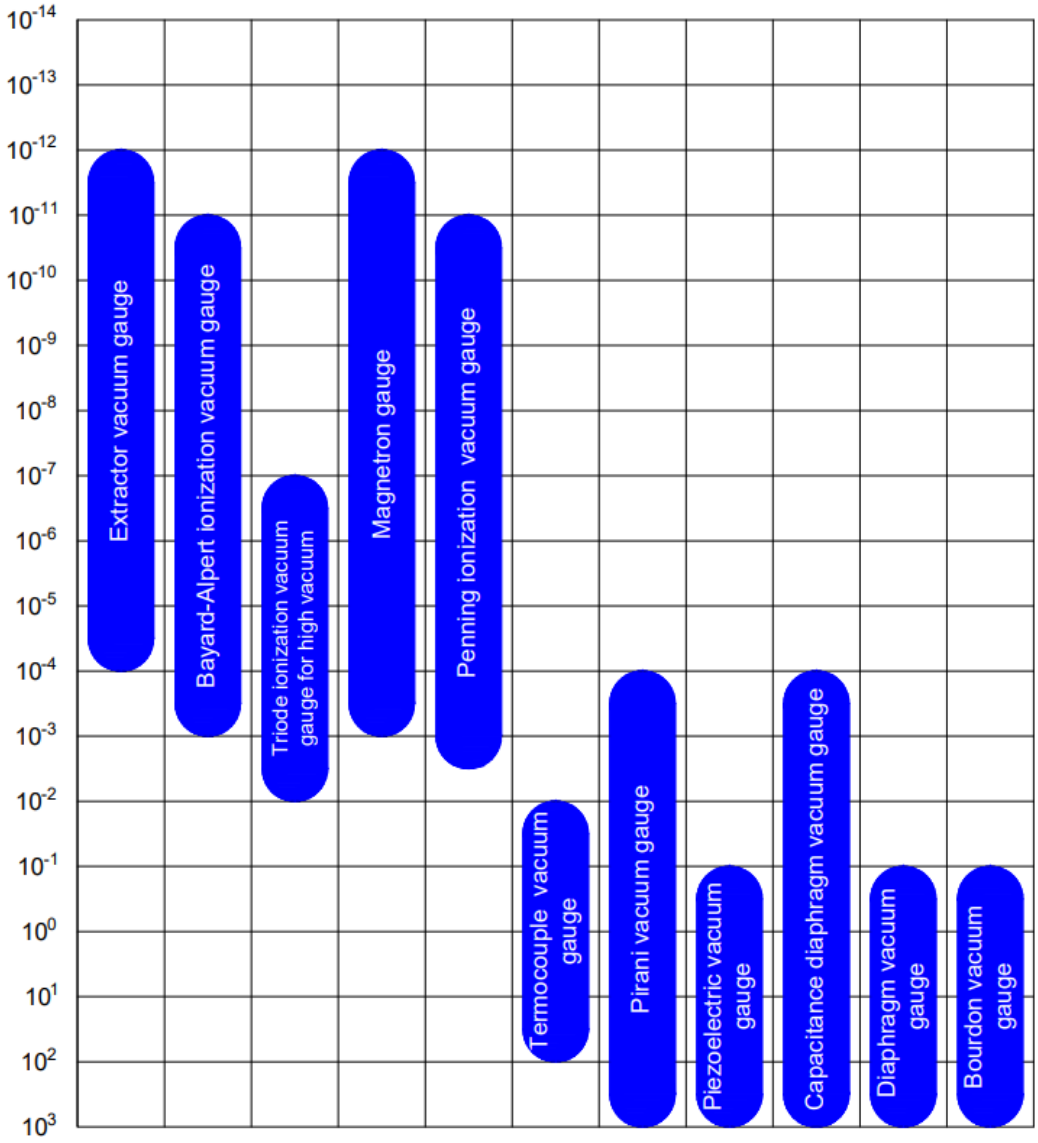


Figure 6. Pressure measurement methods designed to detect different pressure levels [59].

Considering the fact that vacuum technology is constantly evolving and that there is no suitable method to determine the pressure level in extinguishing chambers in real time, the topic has received considerable interest from researchers around the world, resulting in the development of many configurations of measurement systems to detect the pressure level in vacuum apparatus.

3.3. Piezoresistive Sensors for Pressure Measurement

The low-pressure range can be measured using a microelectromechanical systems (MEMS) pressure sensor, which has the advantages of small size, low power requirements, high performance and the possibility of mass production by micromachining. One of the most popular MEMS devices on the industry is pressure sensors. Indeed, it is worth noting that there is a wide range of applications for these sensors, including microscale mechatronic systems, vehicles, aerodynamics, process control and biomedical apparatus [60]. Piezoresistive, capacitive, optical and resonant sensors are just some of the subtypes of

MEMS pressure sensors that can be classified according to sensing principles. Due to their excellent sensitivity, simple design and durability, piezoresistive sensors stand out among them and have been the subject of many studies [61]. In their study, P. Martins et al. tested piezoresistive pressure sensors made by printing technology on ink-based textile substrates and polyethylene terephthalate (PET) [50]. In their work, they demonstrated that, unlike sensors known in industry, the sensors they tested give a linear response. This requires additional verification to confirm the linearity of large-scale operation. S. Kumar and co-workers presented a sensor design on a square diaphragm, which better transmits mechanical stresses, and an amplifier circuit for the above element [51]. Many more piezoelectric sensor designs have been developed in a variety of materials with significant improvements in sensitivity, as shown in Table 4.

Table 4. Chosen piezoresistive sensor designs [52,62–67].

Structure	Sensitivity [kPa^{-1}]
Micro copula	15.10
Micro pyramid	10.30
Micro pillar	2.00
Hierarchical	19.80
Empty crutch	133.10
Textile	14.40

3.4. Fiber Optic Technology in Pressure Measurement

Fiber-optic sensors, such as the Fabry–Perot interferometer (FPI) sensor, Bragg grating (FBG) sensor, polymer FBG sensor and other fiber-optic configurations [68–77] for detecting deformation due to applied pressure, have gained considerable attention from researchers due to their small size, low weight, resistance to electromagnetic interference and high sensitivity. In addition to a number of advantages, fiber-optic technology has the significant disadvantage of being susceptible to temperature effects, so compensation systems are required, and sensors and measurement systems need to be augmented with additional components to measure the reference temperature.

3.4.1. Sensors with a Fabry-Perot Interferometer

The Fabry–Perot interferometer relies on the use of an optical cavity created by placing two optical reflectors M1 and M2 with reflection coefficients R1 and R2 in a specific position on two sides of an optically transparent medium of length h, as shown in Figure 7. The incident light beam produces multiple reflected beams between which interference occurs, giving an interference wave pattern in the spectral domain. The use of IFP in measurements exploits the susceptibility of the pattern to modulation induced by external interference causing changes in refractive index and optical cavity length [78].

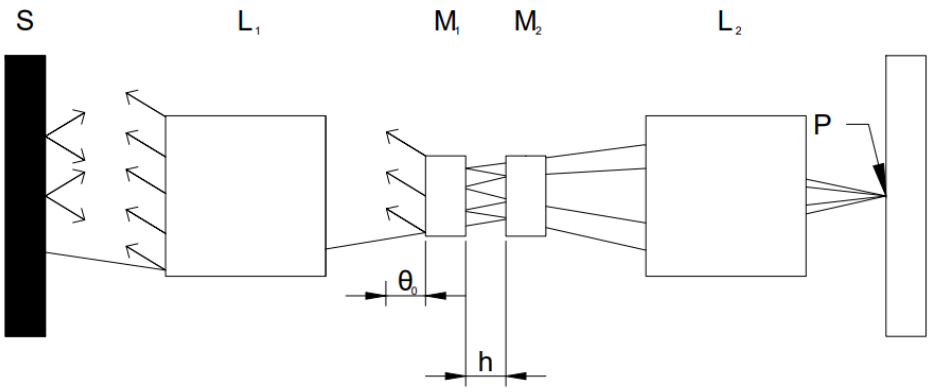


Figure 7. Schematic of the FP cavity [78]. S—source; L_1, L_2—lenses; M_1, M_2—transmissible mirrors; P—point of light on screen; h—distance between mirrors; θ—incidence angle of the wave.

Technology progress has allowed the use of fiber optics as a material for the manufacture of FP sensors. The design of FP interferometers differs depending on the place of use, i.e., for indoor sensors a technology is used where the fiber itself fills the space of the transparent medium (a), while for outdoor designs an air gap or other materials different from the fiber are used (b). The optical gap design for both cases is shown in Figure 8.

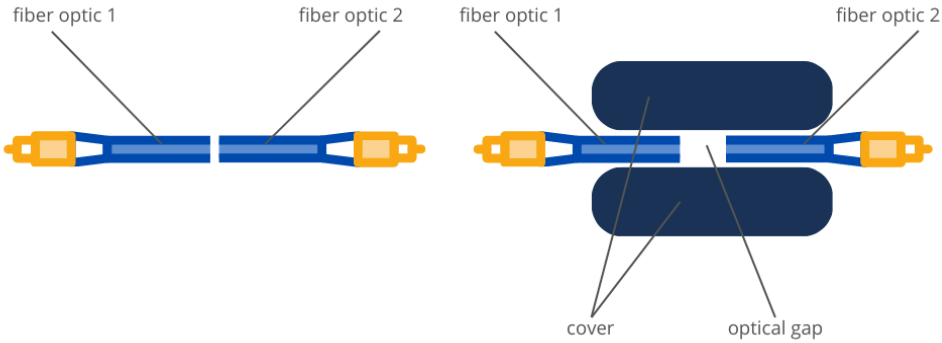


Figure 8. Optical slit structure: (**a**) internal, (**b**) external [78].

Many variants of fiber-optic sensors have been developed to measure, among other things, pressure, which were collected in a book by Y.-J. Rao and others [78]. Other design versions of interferometers are also known. Y.-J. Rao and co-workers presented an FPI made from a hollow photonic core of a bandgap optical fiber [79], J. Villatoro and others developed a version made from a solid photonic core of a crystalline optical fiber [80]. The problem of the former is the need to coat the fiber face, which is complex and expensive, while the latter has questionable stability due to air holes through which the system is even more vulnerable [81]. C. Wu and co-workers developed a high-pressure and high-temperature Fabry–Perot interferometer [82], proving its correct operation up to pressures of the order of 4×10^3 kPa, with an accuracy of 5.8×10^{-3} pm/kPa. W. Wang et al. developed a pressure sensor design capable of measuring from 0 to 50 kPa with an accuracy of 5.3×10^3 pm/kPa [83]. Recent studies show the use of the Mach–Zehnder interferometer [84] and the Sagnac interferometer [85]; however, due to the need for precise positioning of the interferometer components and the relatively complex structure, they have disadvantages in practical application in operation. A summary of selected fiber-optic methods designed for pressure detection is shown in Table 5.

The table shows that, of the presented sensors, the best method is the cascaded FP interferometer in a glass capillary tube, characterized by the highest sensitivity and the lowest temperature influence on the measurement, but the production of the above sensor using a femtosecond laser is technologically complicated and expensive, which poses a serious problem for the commercialization of this technology. A consensus between price and ease of fabrication appears to be the parallel combination of an FP interferometer with an HCF, but this technology requires further research and verification of the sensor's performance under operational conditions.

3.4.2. Sensors with Bragg Gratings

Fiber optic Bragg gratings have gained widespread use in pressure sensing systems, as reflected in many scientific papers. An optical Bragg grating is a periodic structure with a variable refractive index formed in the core of an optical fiber by treating it with UV light. The operation of the grating can be likened to that of a band-stop filter in the transmission operating state [96]. The structure, with its variable refractive parameter, reflects specific wavelengths that do not differ from the wavelengths for the Bragg resonance, and transmits the others without interfering with the passing signal. A schematic of a fiber-optic Bragg grating is shown in Figure 9.

Table 5. Overview of different fiber optic gas pressure sensors [61,83,86–103].

Sensor Type	Sensitivity [pm/kPa]	Temperature Crossover [kPa/°C].	Range of Linear Response [kPa]	Production Type
Anti-resonance sensor with open side channel	4.24	-	0–2 × 10^3	Famtosecond laser
Anti-resonance guiding mechanism with hollow fiber reflection (HCF)	3.59	7.5	0–2 × 10^3	Famtosecond laser
Single FP interferometer with silica membrane	1.036	0.96	0–2 × 10^3	Shell
FP double cavities with composite membrane	30.2	-	0–0.4 × 10^3	Shell
MZ cascade interferometer with myctro-machined air cavity	82.131	0.647	0–0.7 × 10^3	Famtosecond laser
Cascade FP interferometer in a glass capillary tube	86.64	5.18	0–0.6 × 10^3	Famtosecond laser
Parallel connection of the FP interferometer to the gas well	47.76	5.1	0–0.45 × 10^3	Famtosecond laser
FP and Sagnac interferometer separated by silver foil	31.73	-	0–1.6 × 10^3	Shell
Parallel connection of FP interferometers with thin UV adhesive layer	38.3	-	0.1–0.7 × 10^3	Shell
Equivalent combination of FP interferometer with HCF	45.76	0.097	0–3 × 10^3	Arc discharge

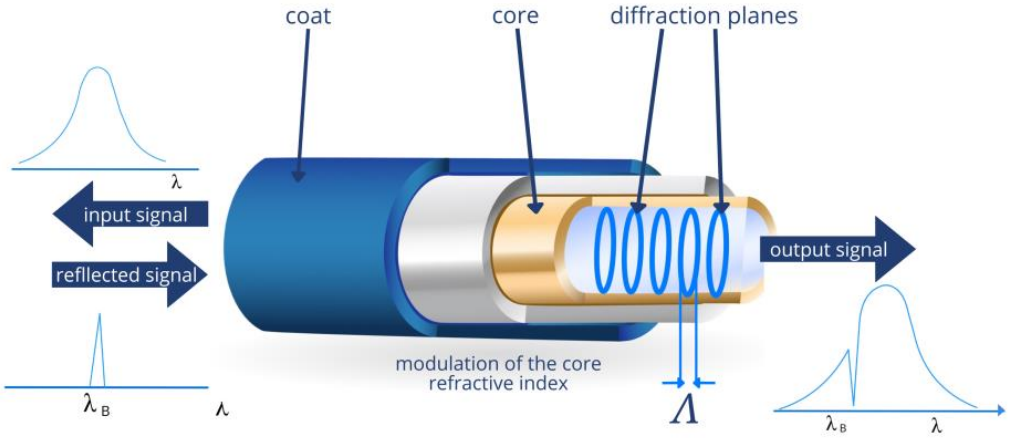


Figure 9. Optical Bragg grating structure [96].

An unframed FBG pressure sensor with a sensitivity of 3.04 × 10^{-3} pm/kPa was first described by M. Xu and co-workers [97], which is a low value for practical pressure measurement. Pressure sensitivity has been improved over the years by experimenting with different housing designs and fabrication technologies. An improved FBG pressure sensor with a sensitivity of 1.414 pm/kPa constructed by J. Huang and co-workers [98] was introduced. It uses a Bourdon tube as the pressure-treated element. M. Liang et al. [93] developed a circular membrane–cantilever pressure sensor based on FBG, which uses two grids glued to the surface of the beam. However, the sensitivity of 0.34 pm/kPa is far below the preferred range, in practical measurements. Developed by J. Huang et al. [99], a fiber-optic sensor had a pressure sensitivity of 1.57 pm/kPa. The inhomogeneity of the Bragg grating stress due to its adhesion to the surface of the circular membrane remains a

problematic issue, which negatively affects the accuracy and reliability of the measurement. The FBG pressure sensor based on a circular membrane was designed by V. Pachava and co-workers [100]. The measured sensitivity of the sensor was quite high at 32.02 pm/kPa. Although, in general, the sensor design is robust the core used is brittle and fails. In addition, the effect of temperature on the pressure measurement was not eliminated by the single Bragg grating in the actual applications. Due to the FBG's simultaneous sensitivity to strain and external temperature, temperature compensation methods that isolate the wavelength shift caused by temperature in FBG pressure sensors are crucial. The pressure sensitivity coefficient of two FBG pressure sensors bonded to the same production materials is comparable, as reported by F. Gu et al. [101]. Both pressure and temperature affect FBG1, but only temperature affects FBG2, which is the reference point. Both FBGs are in the same temperature field and have generally equal center wavelengths. As a result, they are able to produce the same temperature response or the same temperature-induced wavelength shift. By directly comparing the two FBG wavelength shifts, the recorded pressure levels can be determined. Similar to the work of V. Neeharik [102]. Another concept is implemented using twin FBGs whose wavelength shift responds to both temperature and pressure fluctuations as in the paper by E. Vorathin's [103]. A structurally similar variant of this approach described by M. Liang [93] is a reference FBG2 that responds to temperature fluctuations. The two FBGs attached to the structure show the same response to temperature, according to M. Lian and co-workers, the difference being that the external pressure loads in FBG1 were converted to positive strain, while in FBG2 they were converted to negative strain. The difference in wave drift helps remove the effect of temperature from the pressure measurements. The pressure sensor, based on the Leal–Junior et al. membrane, was able to have a reduced transverse sensitivity due to a compensation approach involving the modelling of the sensor [104]. A flexible membrane made of martensitic stainless steel was used by G. Hegde and co-workers [105] to create a sensor with a temperature-compensated fiber Bragg grating. The temperature-compensated FBG mesh was then bonded to a stress-free area of the same flexible membrane. The experimental results show that the pressure sensitivity of the sensor was 3.64 pm/bar. A temperature sensor with a circular membrane was developed by L. Wang with his team [106] using metallised optical fibers. The team focused on the resolution and precision of the sensor, with the temperature accuracy reaching 0.1%, although no temperature compensation methods were used. The square diaphragms, steel trusses and vertical beams were used in the design developed by Q. Fan et al. [107] to investigate and propose a pressure sensor. The pressure sensitivity of the sensor was 622.7×10^{-3} pm/kPa and its hysteresis was minimal. Q. Fan and co-workers [108], developed a sensor consisting of a combination of a single square membrane and FBG characterized by high temperature compensation, but its sensitivity was too low. Although high sensitivity was guaranteed by the sensing structures used in the above research work, the small design made it difficult to eliminate hysteresis or maintain high sensitivity for better temperature compensation effects. Z. Liu et al. [109] developed a square membrane sensor coupled to a lever structure with a sensitivity of 3.35 pm/kPa. A comparison of selected fiber optic sensors is given in Table 6.

Analyzing the table above, it can be seen that by far the best pressure sensitivity was the sensor developed by E. Vorathin and co-workers. This sensor achieved a pressure sensitivity of 100.7 pm/kPa, with a mean square error of 0.1976 kPa. It should be borne in mind that, apart from the pressure and temperature ranges and pressure sensitivity, E. Vorathin does not specify the parameters of the developed sensor, such as repeatability or measurement hysteresis, so it needs to be analyzed in more detail, but by classifying the presented sensor in terms of pressure sensitivity, it provides a good development basis for the design of a pressure measurement sensor for electrical apparatus.

Table 6. Comparison of selected sensors with Bragg gratings [93,99–109].

Parameters	Construction by Q. Fan [108]	Construction by J. J. Huang [99]	Construction by M. Liang [93]	Construction by V. Pachav [100]	Construction by F. Gu [101]	Construction by Q. Fan [108]	Construction by Vorathin [103]	Construction by G. Hegde [105]	Construction by L. Wang [106]
Pressure range	0–200 kPa	0–1 × 10^3 kPa	0–10 × 10^3 kPa	0–207 kPa	0–16 × 10^3 kPa	0–2 × 10^3 kPa	0–10 kPa	0.4–70 × 10^3 kPa	0–1000 kPa
Temperature range	20–55 °C	20–90 °C	5–70 °C	-	25–65 °C	-	27.5–52.5 °C	−40–90 °C	1–35 °C
Pressure sensitivity	3.402 pm/kPa	1.57	0.34	31.9	6.94 × 10^{-2} pm/kPa	6.227 × 10^{-1} pm/kPa	1.007 × 10^2 pm/kPa	3.64 × 10^{-2} pm/kPa	1.611 pm/kPa
Resolution	6.26 kPa	-	-	-	2.88 × 10^{-4} kPa	-	-	-	-
Hysteresis	1.09%	-	-	-	-	0.66%	-	0.75%	-
Repeatability	98.80%	99.40%	-	99.91%	99.71%	99.72%	-	99.98%	99.98%
Pressure measurement error	5.53 kPa	17.2 kPa	92 kPa	-	-	1.46 kPa	-	12.6 kPa	-

3.5. Measurement of Partial Discharge

A variety of detection methods have been investigated to track partial discharge (WNZ) activity, including electrical charge pulses, chemical changes, acoustic wave emissions and electromagnetic wave radiation. There are a variety of sensors and signal processing techniques that can be used to monitor and investigate corona discharges. International Electrotechnical Commission (IEC) 60270 standards and other unconventional methods have been developed and used to test for partial discharges in a number of ways to ensure adequate monitoring performance. Depending on the method of assessment, these techniques can be classified as offline or online detection techniques. Online monitoring, as opposed to offline monitoring, is becoming more common as it causes less system disruption and power outages [110].

Given the need to develop a reliable real-time pressure monitoring system, the attention of researchers has been directed to the measurement of incomplete discharges as a solution that shows great potential toward determining the pressure in gas-insulated switchgear. The idea of the measurement is based on the incomplete discharge occurs between the floating shield in the closed state and between the contacts in the open state, and the measurement of the amount of these discharges depending on the given pressure, through a coupling capacitor connected to the shield inside the chamber [53]. Research conducted by the researchers, proved that there is a relationship between the number of discharges and the pressure level in the apparatus, which is a promising method for indirect pressure measurement in gas-insulated devices. Typical methods of detection of incomplete discharges are shown in Figure 10.

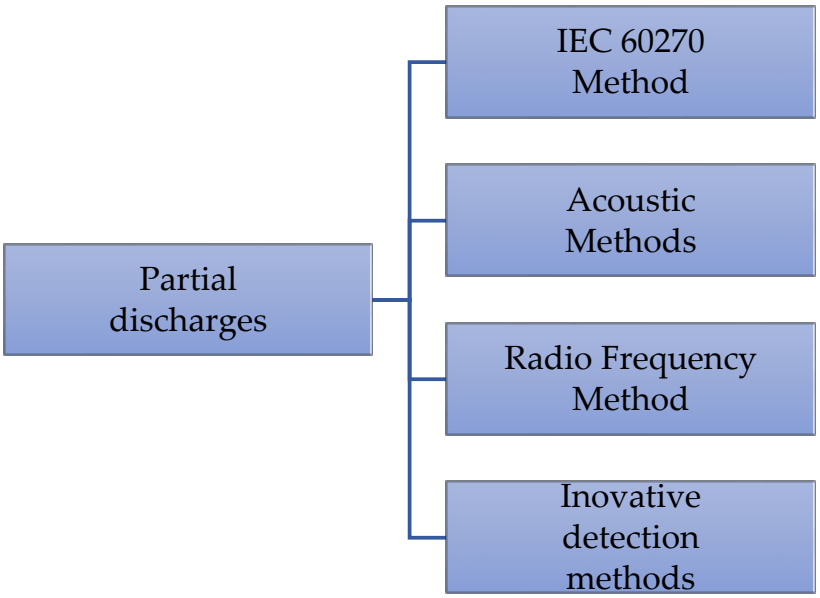


Figure 10. Methods for detecting partial discharges [110].

3.5.1. IEC 60720 Method

IEC 60720 standards are well known for their accuracy and ability to monitor the level of partial discharge in unplugged environments. The basic elements of the test element circuit (C_x), the coupling capacitors (C_b) and the measurement impedance (Z) are shown in Figure 11 as a test circuit for this technique.

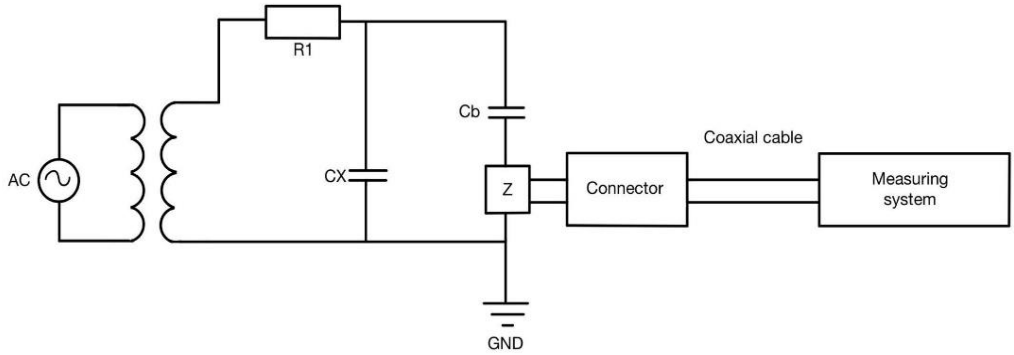


Figure 11. Test circuit for partial discharges [110].

A coupling capacitor can be used to record current pulses below 1 megahertz (MHz), which are caused by partial discharge activity in the test element and connect them to the measurement impedance. The signal can be presented in both time domain and phase domain to highlight the characteristics of the occurrence of partial discharges. There are two different patterns of partial discharge activity that show the relationship between discharge amplitude (q) and number of cycles (n). In terms of phase position (φ), the first are phase-separated partial discharges (PRPD) and phase-separated pulse sequences (PRPS). These were proposed by Fruth in 1990 and are mainly based on statistical considerations to illustrate the characteristic style of several types of damage caused by partial discharges. The three types of partial discharge patterns are surface discharge, hollow discharge and corona discharge. These patterns can be characterized on the basis of prior contributions thanks to data from q-n-φ representations [111]; however, a significant drawback of PRPD and PRPS is their inability to distinguish between source types when several defect types are present and overlapping information in the phase domain can seriously affect the performance of partial discharge classification. To address the challenges of implementing monitoring remotely using IEC 60270 methodologies, researchers have looked at different ways of continuously monitoring detection methods in high-voltage equipment [112]. An actual pole insulator with a microcrack defect was used in an experiment that was conducted by J. Cheng [113]. For a comprehensive study, the radio frequency signal and important parameters based on IEC 60270 standards were measured simultaneously. The results showed that sub-millimeter cracks could occur in the GIS insulator.

3.5.2. Acoustic Method

Acoustic emission is often observed in discharge processes due to the large vibrations of the electrons, and the sampling frequency for acoustic emission detection is 20 kHz–1 MHz. Due to its advantages, such as low sensitivity to electrical noise and the ability to detect discharge places, the acoustic approach is used in partial discharge monitoring systems [114]. Piezoelectric sensors can be installed externally for online monitoring of the appearance of partial discharges without losing power. Solid and liquid insulation, internal insulation and external design of operating equipment tend—in a good way—to influence the propagation characteristics. The solid, liquid and internal insulation of the operating equipment can have a positive effect on thermal propagation. Additionally, depending on the length between the sensors and the source of the partial discharge, the acoustic attenuation can be quite significant [110]. The acoustic way of estimating partial discharges is related to the conventional electrical way, in which partial discharges are measured under different conditions using AET. H. D. Ilkhechi and M. H. Samimi in their work [115] analyzed acoustic approaches and acoustic-electrically coordinated detectors for partial discharges.

3.5.3. Radio Frequency Method

In the case of partial discharges, the radio frequency (RF) method uses matched sensor equipment to distinguish and collect the electromagnetic signal created. On the other hand,

this can reveal the occurrence of partial discharges rather than their exact position. In the meantime, due to its noise immunity and localization accuracy, the UHF procedure is commonly used to inspect sources of partial discharges [110]. Since the measurement frequency is between 300 MHz and 3 GHz, which is above the electronic value, the UHF method has an excellent signal-to-noise ratio. UHF detectors (radio wires) are placed in equipment using oil valves or dielectric windows to collect UHF signals. An interesting concept was presented by Y. Wang and his team [116]. They developed a fiber-optic ultrasonic system for the detection of partial discharges. In order to overcome the problem of the influence of electromagnetic interference on the measurement results, they proposed to use a fiber-optic Sagnac interferometer for ultrasonic detection of partial discharges. The design of the system is not complicated, but detection of partial discharges may not be sufficient for industrial applications mainly due to the accumulation of live components, for example in a vacuum circuit breaker. This can lead to detection of discharges from the wrong current path, or even to detection of a partial discharge in the device, but without being able to determine the specific location of the discharge.

3.5.4. Other Innovative Measurement and Detection Methods

Y. Nakano and co-authors [117] investigated the characteristics of partial discharges in the medium vacuum range in air and SF_6 gas as a leakage gas for a vacuum stage diagnosis method. A detection resistor attached to a grounded flat electrode outside the device can detect the partial discharge. From the acquired charges, the team determined the incidence and phase characteristics of the discharges for the applied AC voltage, as well as the internal pressure of the vacuum. The internal pressure of the device can be determined by statistical analysis of the discharge occurrence histogram for its phase, but these results can only be applied to a device with the same geometry and voltage rating.

C.-J. Chou and C.-H. Chen [118] in their research have introduced a measurement method using a high-frequency current transformer (HFCT), and then modelled various partial discharges, including internal discharges, discharges along the surface and discharges at the ends of conductors. In addition, they analyzed the characteristics of the discharge waveform and phase distribution to identify the type of partial discharge. The measured and analyzed results for the real case are compared with standard discharge pattern data from the laboratory. This can form the basis for a database of partial discharges in medium-voltage power equipment, which is also required for the development of an automatic partial discharge identification system.

H.-B. Su and others [119] have presented a technique for monitoring the degree of vacuum remotely in high voltage vacuum circuit breakers (HVVCBs) together with a data processing circuit. In order to receive the electromagnetic signal produced by the pulse discharge, a ring antenna is placed on the vicinity of the vacuum breaker. The electromagnetic signal must then be converted into an electrical signal and sent to the circuit for processing and treatment. The system, after filtering the signal, pre-amplifies it by a certain multiple and keeps track of the number of pulse signals processed and the average amplitude of the signal over 30 s for each vacuum level. A relay is then triggered according to the selected threshold amplitude values and number of signals to signal that the threshold parameter has been exceeded. Measurement by this method is possible without interfering with the design of the device, but requires the use of an antenna, the location of which can be problematic, particularly in operational applications, and the pressure values obtained by this method are in the order of 1 Pa, so there is the possibility of detecting system leakage.

So Yeon Kim and a research group [120] have compared the partial discharge characteristics of SF_6 and dry air, showing that there are no significant differences in the propagation of partial discharges which allows the interchangeable use of identical corona discharge sensors for both sulphur hexafluoride and dry air.

Nam-Hoon Kim et al. [121] studied the characteristics of partial discharges in g3 gas and dry air and compared them to SF_6. They showed that hexafluoride sulphur had better insulating properties, with g3 showing about 80% of the insulating capacity of SF_6.

S. Bang and co-workers [55] have described a method for pressure determination based on partial discharges achieving pressure detection of 10^{-2} Pa. The measurement was performed using an LDS-6 partial discharge analyzer from Doble Lemke Co. The system is promising; however, the number of components required is problematic during operational applications.

In another paper, S. Bang and others [122] have compared partial discharges taking place at AC and DC voltages for positive and negative polarity. They used an LDS-6 analyzer for the detection of partial discharges. They proposed maintenance standards depending on the voltage type, monitored the vacuum level in the distribution class and compared AC and DC partial discharges. According to the voltage type, the vacuum level at which the dielectric resistance drops rapidly was validated for proper device operation. In addition, a coupling capacitor was mounted directly on the floating cover of the apparatus to improve the precision of the partial discharge signal detection. The PRPD for the AC partial discharge and the PSA for the DC partial discharge were used to measure the pattern and apparent charge of the partial discharge with respect to the degree of vacuum. The work carried out by S. Bang and co-workers is well suited to testing vacuum chambers for transmission voltages but can be problematic to use in operation.

W. I. Wang, with co-workers [123], has developed a method to determine the degree of vacuum in the apparatus based on continuous wave terahertz imaging. They observed that the signal intensity of the echo spectrum is inversely proportional to the degree of vacuum in the chamber. Which makes it possible to conclude that as the degree of vacuum increases, the amplitude attenuation effect of the detected terahertz signal is gradually weakened, and the time delay is reduced. It shows that the spectrum and absorption spectrum obtained by continuous wave terahertz imaging technology can sensitively distinguish the pressure change in the vacuum environment.

A. Caprara and others [124] have implemented measurement techniques from high-voltage systems into medium-voltage equipment. The use of the Rogowski coil together with the RFCT sensor allowed them to show that the partial discharge detector, thanks to its ability to track individual phenomena, is not affected by the false positive warnings typical of current technologies available for online partial discharge monitoring of distribution networks.

I.-H. Chung [125], in his research, has described the application of a neuro-fuzzy inference system to identify defects in gas-insulated equipment based on partial discharges. He subjected 17 parameters characteristic of corona discharges to analysis. He achieved the system's ability to detect device defects at a level of 90%; however, a comprehensive database is required for the verification accuracy to be at an adequate level, for the system to give more accurate defect detection results in practical applications, and for the stability of system operation to improve.

4. Summary

The article analyses and compares the degree of knowledge in the field of monitoring and diagnosing the condition of gas-insulated electrical equipment in the context of determining the pressure values prevailing in vacuum extinguishing chambers in switching apparatus. The significant technological advances that have taken place in recent years have resulted in a plethora of technological solutions to improve the speed and accuracy of pressure measurements in gas-insulated switchgear, but despite all efforts, there are still a number of issues that need to be clarified and that require further experimental work. One of these is real-time pressure measurement, as most measurement methods are geared towards measuring overpressure, which is not applicable to switchgear that is based on high vacuum. To the knowledge of the research group, which includes the authors of the above document, there is no technological solution for continuous pressure measurement

designed for equipment that is continuously in operation. This leaves a lot of space for research and development work to enable the development of an online vacuum chamber diagnostic system. The most promising methods are associated with the use of fiber optic techniques due to their small size, low weight, resistance to electromagnetic interference and high sensitivity. Current research makes it possible to claim that the development of measurement and diagnostic methods for both vacuum chambers and the target vacuum apparatus will be closely linked to information technology, making it possible to create an autonomous system for monitoring the parameters of electrical apparatus with little operator intervention.

Author Contributions: P.W. proposed the topic and problem area of the article; D.K. and M.L. reviewed, compared and contrasted the state of knowledge on vacuum sensors and wrote the paper; P.W. revised the paper and contributed to the discussion increasing the merit of the paper. All authors have read and agreed to the published version of the manuscript.

Funding: This research received no external funding.

Data Availability Statement: Not applicable.

Acknowledgments: This work was supported by The National Centre for Research and Development and co-financed from the European Union funds under the Smart Growth Operational Programme (grant # POIR.01.01.01-00-0451/21).

Conflicts of Interest: The authors declare no conflict of interest.

References

1. Colak, I.; Bayindir, R.; Sagiroglu, S. The Effects of the Smart Grid System on the National Grids. In Proceedings of the 2020 8th International Conference on Smart Grid (icSmartGrid), Paris, France, 17–19 June 2020; pp. 122–126. [CrossRef]
2. The EU in the World-Energy-Statistics Explained. Available online: https://ec.europa.eu/eurostat/statistics-explained/index.php?title=The_EU_in_the_world_-_energy#Electricity_generation (accessed on 11 August 2022).
3. Mohanty, S.P.; Choppali, U.; Kougianos, E. Everything you wanted to know about smart cities: The Internet of things is the backbone. *IEEE Consum. Electron. Mag.* **2016**, *5*, 60–70. [CrossRef]
4. Morello, R.; de Capua, C.; Fulco, G.; Mukhopadhyay, S.C. A Smart Power Meter to Monitor Energy Flow in Smart Grids: The Role of Advanced Sensing and IoT in the Electric Grid of the Future. *IEEE Sens. J.* **2017**, *17*, 7828–7837. [CrossRef]
5. VD4-Medium Voltage Vacuum Circuit-Breakers. Available online: https://search.abb.com/library/Download.aspx?DocumentID=1VCP000001_A&LanguageCode=pl&DocumentPartId=&Action=Launch (accessed on 28 November 2022).
6. Totally Integrated Power-SION Wyłączniki Próżniowe SION Typu 3AE5 i 3AE1 Aparaty Łączeniowe Średniego Napięcia. Available online: https://publikacje.siemens-info.com/pdf/115/Wy%C5%82%C4%85czniki%20pr%C3%B3%C5%BCniowe%20SION.pdf (accessed on 8 September 2022).
7. Slade, P.G. *The Vacuum Interrupter*, 2nd ed.; CRC Press: Boca Raton, FL, USA, 2020. [CrossRef]
8. Alsumaidaee, Y.; Yaw, C.; Koh, S.; Tiong, S.; Chen, C.; Ali, K. Review of Medium-Voltage Switchgear Fault Detection in a Condition-Based Monitoring System by Using Deep Learning. *Energies* **2022**, *15*, 6762. [CrossRef]
9. Yeckley, R.; Perulfi, J. Oil circuit breakers: A look at the earlier generation [history]. *IEEE Power Energy Mag.* **2018**, *16*, 86–97. [CrossRef]
10. Pei, X.; Cwikowski, O.; Vilchis-Rodriguez, D.S.; Barnes, M.; Smith, A.C.; Shuttleworth, R. A review of technologies for MVDC circuit breakers. In Proceedings of the IECON 2016—42nd Annual Conference of the IEEE Industrial Electronics Society, Florence, Italy, 23–26 October 2016; pp. 3799–3805. [CrossRef]
11. Park, W.; Kim, Y.K.; Lee, S.; Ahn, K.-Y.; Kim, Y.-G. Arc phenomena and method of arc extinction in air circuit breaker. In Proceedings of the 25th International Conference on Electricity Distribution (CIRED 2019), Madrid, Spain, 3–6 June 2019.
12. Air Circuit Breaker: Construction, Types, Working & Its Applications. Available online: https://www.elprocus.com/air-circuit-breaker-acb-working-principle-application/ (accessed on 12 November 2022).
13. Tian, S.; Zhang, X.; Xiao, S.; Zhang, J.; Chen, Q.; Li, Y. Application of $C_6F_{12}O/CO_2$ mixture in 10 kV medium-voltage switchgear. *IET Sci. Meas. Technol.* **2019**, *13*, 1225–1230. [CrossRef]
14. Seeger, M.; Smeets, R.; Yan, J.; Ito, H.; Claessens, M.; Dullni, E.; Falkingham, L.; Franck, C.M.; Gentils, F.; Hartmann, W.; et al. Recent Trends in Development of High Voltage Circuit Breakers with SF6 Alternative Gases. *Plasma Phys. Technol.* **2017**, *4*, 8–12. [CrossRef]
15. Xemard, A.; Jurisic, B.; Rioual, M.; Olivier, A.; Sellin, E. Interruption of small, medium-voltage transformer current with a vacuum circuit breaker. *Electr. Power Syst. Res.* **2020**, *187*, 106502. [CrossRef]
16. Moore, T.; Schmid, F.; Tricoli, P. Voltage transient management for Alternating Current trains with vacuum circuit breakers. *IET Electr. Syst. Transp.* **2021**, *12*, 1–14. [CrossRef]

17. Węgierek, P.; Staszak, S.; Pastuszak, J. EKTOS—Innowacyjny napowietrzny rozłącznik próżniowy średniego napięcia w obudowie zamkniętej przeznaczony do sieci smart grids. *Wiadomości Elektrotechniczne* **2019**, *1*, 23–27. [CrossRef]
18. Węgierek, P.; Lech, M.; Kostyła, D.; Kozak, C. Study on the Effect of Helium on the Dielectric Strength of Medium-Voltage Vacuum Interrupters. *Energies* **2021**, *14*, 3742. [CrossRef]
19. Slade, P.G. *The Vacuum Interrupter*, 1st ed.; CRC Press: Boca Raton, FL, USA, 2018. [CrossRef]
20. United Nations. *Kyoto Protocol to the United Nations Framework Convention on Climate Change*; United Nations: Rome, Italy, 1998.
21. Kumar, S.; Madlener, R. Energy systems and COP21 Paris climate agreement targets in Germany: An integrated modeling approach. In Proceedings of the 2018 7th International Energy and Sustainability Conference (IESC), Cologne, Germany, 17–18 May 2018; pp. 1–6. [CrossRef]
22. Ullah, R.; Rashid, A.; Rashid, A.; Khan, F.; Ali, A. Dielectric characteristic of dichlorodifluoromethane (R12) gas and mixture with N_2/air as an alternative to SF_6 gas. *High Volt.* **2017**, *2*, 205–210. [CrossRef]
23. Ullah, R.; Ullah, Z.; Haider, A.; Amin, S.; Khan, F. Dielectric properties of tetrafluoroethane (R134) gas and its mixtures with N_2 and air as a sustainable alternative to SF_6 in high voltage applications. *Electr. Power Syst. Res.* **2018**, *163*, 532–537. [CrossRef]
24. Kharal, H.S.; Kamran, M.; Ullah, R.; Saleem, M.Z.; Alvi, M.J. Environment-Friendly and Efficient Gaseous Insulator as a Potential Alternative to SF_6. *Processes* **2019**, *7*, 740. [CrossRef]
25. European Parliament and of the Council. Regulation of the European Parliament and of the Council on Fluorinated Greenhouse Gases. 2022. Available online: https://eur-lex.europa.eu/legal-content/EN/TXT/HTML/?uri=CELEX:52022PC0150 (accessed on 6 October 2022).
26. Zhong, L.; Rong, M.; Wang, X.; Wu, J.; Han, G.; Han, G.; Lu, Y.; Yang, A.; Wu, Y. Compositions, thermodynamicproperties, and transport coefficients of high temperature $C_5F_{10}O$ mixed with CO_2 and O_2 as substitutes for SF_6 to reduce global warming potential. *AIP Adv.* **2017**, *7*, 075003. [CrossRef]
27. Xiao, D. *Gas Discharge and Gas Insulation 6*; Springer: Berlin/Heidelberg, Germany, 2016. [CrossRef]
28. Li, X.; Zhao, H.; Murphy, A.B. SF_6-alternative gases for application in gas-insulated switchgear. *J. Phys. D Appl. Phys.* **2018**, *51*, 153001. [CrossRef]
29. Kovács, T.; Feng, W.; Totterdill, A.; Plane, J.M.C.; Dhomse, S.; Gómez-Martín, J.C.; Stiller, G.P.; Haenel, F.J.; Smith, C.; Forster, P.M.; et al. Determination of the atmospheric lifetime and global warming potential of sulfur hexafluoride using a three-dimensional model. *Atmos. Chem. Phys.* **2017**, *17*, 883–898. [CrossRef]
30. Hosl, A.; Pachin, J.; Eguz, E.; Chachereau, A.; Franck, C.M. Positive synergy of SF6 and HFO1234ze(E). *IEEE Trans. Dielectr. Electr. Insul.* **2020**, *27*, 322–324. [CrossRef]
31. Hopf, A.; Britton, J.A.; Rossner, M.; Berger, F. Dielectric strength of SF6 substitutes, alternative insulation gases and PFC-gas-mixtures. In Proceedings of the 2017 IEEE Electrical Insulation Conference (EIC), Baltimore, MD, USA, 11–14 June 2017; pp. 209–212.
32. Park, D.-W.; Han, S.-H.; Seon, H.S.; Shin, P.-K.; Park, D.W. Conversion of SF 6 by Thermal Plasma at Atmospheric Pressure. Available online: https://www.researchgate.net/publication/268405914 (accessed on 28 November 2022).
33. Ito, H. (Ed.) *Switching Equipment*; Springer International Publishing: Cham, Switzerland, 2019. [CrossRef]
34. Conseil International des Grands RéseauxÉlectriques. *Comité D'études A3. and Impr. Conformes), the Impact of the Application of Vacuum Switchgear at Transmission Voltages*; CIGRÉ: Paris, France, 2014.
35. Yao, X.; Wang, J.; Ai, S.; Liu, Z.; Geng, Y.; Hao, Z. *Vacuum Switching Technology for Future of Power Systems. Engineering*; Elsevier Ltd.: Amsterdam, The Netherlands, 2022. [CrossRef]
36. Duan, X.; Li, F.; Dong, E.; Liao, M.; Guo, Y.; Zou, J. Study on Inner Vacuum Pressure Measurement System of Vacuum Circuit Breakers. In Proceedings of the 2017 4th International Conference on Electric Power Equipment-Switching Technology (ICEPE-ST), Xi'an, China, 22–25 October 2017.
37. Mei, Y.; Yuan, H.; Wang, X.; Sha, K.; Wang, P.; Guo, J.; Xu, W.; Rong, M.; Wang, W. Study on the change tendency of electro-magnetic signal under different vacuum degree for 10 kV vacuum chamber. In Proceedings of the TENCON 2015—2015 IEEE Region 10 Conference, Macao, China, 1–4 November 2015; pp. 1–6. [CrossRef]
38. Yao, X.; Wang, J.; Geng, Y.; Liu, Z.; Zhai, X. Determination of opening velocities for vacuum circuit breakers at transmission voltage. In Proceedings of the 2016 27th International Symposium on Discharges and Electrical Insulation in Vacuum (ISDEIV), Suzhou, China, 18–23 September 2016; pp. 1–4. [CrossRef]
39. Zhang, B.; Ren, L.; Ding, J.; Wang, J.; Liu, Z.; Geng, Y.; Yanabu, S. A Relationship Between Minimum Arcing Interrupting Capability and Opening Velocity of Vacuum Interrupters in Short-Circuit Current Interruption. *IEEE Trans. Power Deliv.* **2018**, *33*, 2822–2828. [CrossRef]
40. Heinz, T.; Koletzko, M.; Giere, S.; Wenzel, N.; Wethekam, S. Control of Vacuum Arcs in High-Voltage Vacuum Interrupters by Suitable Stroke Trajectories of Opening AMF Contacts. In Proceedings of the 2018 28th International Symposium on Discharges and Electrical Insulation in Vacuum (ISDEIV), Greifswald, Germany, 23–28 September 2018; pp. 535–538. [CrossRef]
41. Sun, L.; Yu, L.; Liu, Z.; Wang, J.; Geng, Y. An Opening Displacement Curve Characteristic Determined by High-Current Anode Phenomena of a Vacuum Interrupter. *IEEE Trans. Power Deliv.* **2013**, *28*, 2585–2593. [CrossRef]
42. Duan, X.; Sun, Q.; Wang, W.; Li, J.; Zhang, L.; Dong, E.; Zhu, Y. Design and Dynamic Performance Analysis of Brushless DC Motor Operating Mechanism for UHV Bypass Switch. In Proceedings of the 2019 4th International Conference on Mechanical, Control and Computer Engineering (ICMCCE), Hohhot, China, 24–26 October 2019; pp. 146–1463. [CrossRef]

43. Fang, S.; Xia, M.; Lin, H.; Ho, S. Analysis and design of a high-speed permanent magnet characteristic actuator using eddy current effect for high-voltage vacuum circuit breaker. *IET Electr. Power Appl.* **2016**, *10*, 268–275. [CrossRef]
44. Bissal, A.; Magnusson, J.; Engdahl, G. Comparison of Two Ultra-Fast Actuator Concepts. *IEEE Trans. Magn.* **2012**, *48*, 3315–3318. [CrossRef]
45. Yao, X.; Guan, C.; Wang, J.; Liu, Z.; Ai, S.; Ma, K.; Ma, F. Technology of AC Short-Circuit Current Controlled Fast Vacuum Breaking in a Short Arcing Time. In Proceedings of the 2020 IEEE International Conference on Applied Superconductivity and Electromagnetic Devices (ASEMD), Tianjin, China, 16–18 October 2020; pp. 1–2. [CrossRef]
46. Stoczko, S.; Szewczyk, M.; Pochanke, Z.; Chmielak, W. Experimental study on field emission current in vacuum interrupter at functional limit of vacuum pressure. *Electr. Power Syst. Res.* **2021**, *191*, 106860. [CrossRef]
47. Lech, M.; Kostyła, D. Metoda określania rzeczywistej wartości ciśnienia w próżniowej komorze gaszeniowej sn. Informatyka, Automatyka. *Pomiary Gospod. Ochr. Sr.* **2021**, *11*, 28–31. [CrossRef]
48. Węgierek, P. Test stand for testing and diagnostics of medium voltage vacuum interrupters. *Przegląd Elektrotechniczny* **2021**, *1*, 178–181. [CrossRef]
49. Komory Próżniowe. Available online: https://proznia.itr.org.pl/komory-prozniowe#gallery-3 (accessed on 12 November 2022).
50. Martins, P.; Silva, C.; Oliveira, J.; Marques, A. Preliminary Tests with Screen-Printed Piezoresistive Pressure Sensors on PET and Textile Substrates. In Proceedings of the 2022 IEEE International Conference on Flexible and Printable Sensors and Systems (FLEPS), Vienna, Austria, 10–13 July 2022; pp. 1–4. [CrossRef]
51. Kumar, S.; Rathore, P.K.; Rangababu, P. Implementation of operational amplifier for the designing of novel piezoresistive pressure sensor. In Proceedings of the 2018 2nd International Conference on Smart Sensors and Application (ICSSA), Kuching, Malaysia, 24–26 July 2018; pp. 126–129. [CrossRef]
52. Pan, L.; Chortos, A.; Yu, G.; Wang, Y.; Isaacson, S.; Allen, R.; Shi, Y.; Dauskardt, R.; Bao, Z. An ultra-sensitive resistive pressure sensor based on hollow-sphere microstructure induced elasticity in conducting polymer film. *Nat. Commun.* **2014**, *5*, 3002. [CrossRef]
53. Bang, S.; Lee, H.W.; Lee, B.W. Real-time monitoring of the vacuum degree based on the partial discharge and an insulation supplement design for a distribution class vacuum interrupter. *Energies* **2021**, *14*, 7891. [CrossRef]
54. Chmielak, W. Review of methods of diagnostics of the vacuum in vacuum circuit breakers. *Przegląd Elektrotechniczny* **2014**, *2*, 213–216. [CrossRef]
55. Yan, F.; Jin, D.; Chen, L.; Wan, X.; Xiao, K. Non-destructive gas pressure measurement in compact sealed electronic vacuum devices by penning-type discharge. In Proceedings of the 2016 27th International Symposium on Discharges and Electrical Insulation in Vacuum (ISDEIV), Suzhou, China, 18–23 September 2016; pp. 1–2. [CrossRef]
56. Kuhl, W.; Schilling, W.; Schlenk, W. Messung des lnnendruckes in Vakuumschaltröhr. *Vakuum-Technik* **1985**, *34*.
57. Vidar_DS_PL. Available online: https://embed.widencdn.net/pdf/plus/megger/2seoiw0prn/Vidar_DS_PL.pdf (accessed on 8 September 2022).
58. Dugan, G.F.; Sonnad, K.G.; Cimino, R.; Ishibashi, T.; Schäfers, F. Measurements of X-ray scattering from accelerator vacuum chamber surfaces, and comparison with an analytical model. *Phys. Rev. Spec. Top.-Accel. Beams* **2015**, *18*, 040704. [CrossRef]
59. How Is Vacuum Pressure Measured—Leybold. Available online: https://www.leybold.com/en/knowledge/vacuum-fundamentals/vacuum-measurement/how-is-vacuum-pressure-measured (accessed on 17 September 2022).
60. Tran, A.V.; Zhang, X.; Zhu, B. The Development of a New Piezoresistive Pressure Sensor for Low Pressures. *IEEE Trans. Ind. Electron.* **2018**, *65*, 6487–6496. [CrossRef]
61. Li, J.; Fang, L.; Sun, B.; Li, X.; Kang, S.H. Review—Recent Progress in Flexible and Stretchable Piezoresistive Sensors and Their Applications. *J. Electrochem. Soc.* **2020**, *167*, 037561. [CrossRef]
62. Jian, M.; Xia, K.; Wang, Q.; Yin, Z.; Wang, H.; Wang, C.; Xie, H.; Zhang, M.; Zhang, Y. Flexible and Highly Sensitive Pressure Sensors Based on Bionic Hierarchical Structures. *Adv. Funct. Mater.* **2017**, *27*, 1606066. [CrossRef]
63. Wang, X.; Gu, Y.; Xiong, Z.; Cui, Z.; Zhang, T. Silk-Molded Flexible, Ultrasensitive, and Highly Stable Electronic Skin for Monitoring Human Physiological Signals. *Adv. Mater.* **2014**, *26*, 1336–1342. [CrossRef]
64. Park, H.; Jeong, Y.R.; Yun, J.; Hong, S.Y.; Jin, S.; Lee, S.-J.; Zi, G.; Ha, J.S. Stretchable Array of Highly Sensitive Pressure Sensors Consisting of Polyaniline Nanofibers and Au-Coated Polydimethylsiloxane Micropillars. *ACS Nano* **2015**, *9*, 9974–9985. [CrossRef]
65. Choong, C.-L.; Shim, M.-B.; Lee, B.-S.; Jeon, S.; Ko, D.-S.; Kang, T.-H.; Bae, J.; Lee, S.H.; Byun, K.-E.; Im, J.; et al. Highly Stretchable Resistive Pressure Sensors Using a Conductive Elastomeric Composite on a Micropyramid Array. *Adv. Mater.* **2014**, *26*, 3451–3458. [CrossRef]
66. Park, J.; Lee, Y.; Hong, J.; Ha, M.; Jung, Y.-D.; Lim, H.; Kim, S.Y.; Ko, H. Giant Tunneling Piezoresistance of Composite Elastomers with Interlocked Microdome Arrays for Ultrasensitive and Multimodal Electronic Skins. *ACS Nano* **2014**, *8*, 4689–4697. [CrossRef]
67. Liu, M.; Pu, X.; Jiang, C.; Liu, T.; Huang, X.; Chen, L.; Du, C.; Sun, J.; Hu, W.; Wang, Z.L. Large-Area All-Textile Pressure Sensors for Monitoring Human Motion and Physiological Signals. *Adv. Mater.* **2017**, *29*, 1703700. [CrossRef]
68. Leal-Junior, A.G.; Díaz, C.A.R.; Frizera, A.; Marques, C.; Ribeiro, M.R.N.; Pontes, M.J. Simultaneous measurement of pressure and temperature with a single FBG embedded in a polymer diaphragm. *Opt. Laser Technol.* **2019**, *112*, 77–84. [CrossRef]
69. Leal-Junior, A.; Campos, V.; Frizera, A.; Marques, C. Low-cost and high-resolution pressure sensors using highly stretchable polymer optical fibers. *Mater. Lett.* **2020**, *271*, 127810. [CrossRef]

70. Leal-Junior, A.; Frizera, A.; Marques, C. A fiber Bragg gratings pair embedded in a polyurethane diaphragm: Towards a temperature-insensitive pressure sensor. *Opt. Laser Technol.* **2020**, *131*, 106440. [CrossRef]
71. Ishikawa, R.; Lee, H.; Lacraz, A.; Theodosiou, A.; Kalli, K.; Mizuno, Y.; Nakamura, K. Pressure Dependence of Fiber Bragg Grating Inscribed in Perfluorinated Polymer Fiber. *IEEE Photonics Technol. Lett.* **2017**, *29*, 2167–2170. [CrossRef]
72. Zhang, Q.; Wang, Y.; Sun, Y.; Gao, L.; Zhang, Z.; Zhang, W.; Zhao, P.; Yue, Y. Using Custom Fiber Bragg Grating-Based Sensors to Monitor Artificial Landslides. *Sensors* **2016**, *16*, 1417. [CrossRef]
73. Luo, Y.-T.; Wang, H.-B.; Ma, G.-M.; Song, H.-T.; Li, C.; Jiang, J. Research on High Sensitive D-Shaped FBG Hydrogen Sensors in Power Transformer Oil. *Sensors* **2016**, *16*, 1641. [CrossRef]
74. He, X.; Ma, C.; Wang, X.; Wang, Z.; Yuan, L. Pressure vector sensor based on an orthogonal optical path Sagnac interferometer. *Opt. Express* **2020**, *28*, 7969. [CrossRef]
75. Paixão, T.; Araújo, F.; Antunes, P. Highly sensitive fiber optic temperature and strain sensor based on an intrinsic Fabry–Perot interferometer fabricated by a femtosecond laser. *Opt. Lett.* **2019**, *44*, 4833. [CrossRef]
76. Qi, Y.; Zhang, J.; Feng, Q.; Zhang, X.; Liu, Y.; Han, Y. A Novel High Sensitivity Refractive Index Sensor Based on Multi-Core Micro/Nano Fiber. *Photonic Sens.* **2019**, *9*, 197–204. [CrossRef]
77. Lin, H.; Liu, F.; Guo, H.; Zhou, A.; Dai, Y. Ultra-highly sensitive gas pressure sensor based on dual side-hole fiber interferometers with Vernier effect. *Opt. Express* **2018**, *26*, 28763. [CrossRef]
78. Rao, Y.-J.; Ran, Z.-L.; Gong, Y. *Fiber-Optic Fabry–Perot Sensors*; CRC Press, Taylor & Francis Group: Boca Raton, FL, USA, 2017. [CrossRef]
79. Rao, Y.J.; Zhu, T.; Yang, X.C.; Duan, D.W. In-line fiber-optic etalon formed by hollow-core photonic crystal fiber. *Opt. Lett.* **2007**, *32*, 2662–2664. [CrossRef]
80. Villatoro, J.; Finazzi, V.; Coviello, G.; Pruneri, V. Photonic-crystal-fiber-enabled micro-Fabry–Perot interferometer. *Opt. Lett.* **2009**, *34*, 2441–2443. [CrossRef]
81. Villatoro, J.; Kreuzer, M.P.; Jha, R.; Minkovich, V.P.; Finazzi, V.; Badenes, G.; Pruneri, V. Photonic crystal fiber interferometer for chemical vapor detection with high sensitivity. *Opt. Express* **2009**, *17*, 1447–1453. [CrossRef]
82. Wu, C.; Fu, H.Y.; Qureshi, K.K.; Guan, B.-O.; Tam, H.Y. High-pressure and high-temperature characteristics of a Fabry–Perot interferometer based on photonic crystal fiber. *Opt. Lett.* **2011**, *36*, 412. [CrossRef]
83. Wang, W.; Li, F. Large-range liquid level sensor based on an optical fibre extrinsic Fabry–Perot interferometer. *Opt. Lasers Eng.* **2014**, *52*, 201–205. [CrossRef]
84. Lin, H.; Liu, F.; Dai, Y.; Zhou, A. Cascaded Fiber Mach–Zehnder Interferometers for Sensitivity-Enhanced Gas Pressure Measurement. *IEEE Sens. J.* **2019**, *19*, 2581–2586. [CrossRef]
85. Qi, Y.; Cong, B.; Liu, Z.; Gong, C.; Li, F.; Hu, T.; Liu, Y. All-fiber sensitivity-enhanced pressure sensor based on Sagnac and F-P interferometer. *Optik* **2021**, *243*, 167359. [CrossRef]
86. Pan, R.; Yang, W.; Li, L.; Yang, Y.; Yu, X.; Fan, J.; Yu, S.; Xiong, Y.; Zhang, L. High-sensitive fiber-optic pressure sensor based on Fabry-Perot interferometer filled with ultraviolet glue film and Vernier effect. *Opt. Fiber Technol.* **2021**, *67*, 102710. [CrossRef]
87. Guo, X.; Ye, W.; Jiang, C.; Sun, S. High sensitivity gas pressure sensor based on two parallel-connected Fabry–Perot interferometers and Vernier effect. *Meas. Sci. Technol.* **2021**, *32*, 125124. [CrossRef]
88. Chen, P.; Dai, Y.; Zhang, D.; Wen, X.; Yang, M. Cascaded-Cavity Fabry-Perot Interferometric Gas Pressure Sensor based on Vernier Effect. *Sensors* **2018**, *18*, 3677. [CrossRef]
89. Wang, J.; Li, L.; Liu, S.; Wu, D.; Wang, W.; Song, M.; Wang, G.; Huang, M. Investigation of Composite Structure with Dual Fabry–Perot Cavities for Temperature and Pressure Sensing. *Photonics* **2021**, *8*, 138. [CrossRef]
90. Liao, C.; Liu, S.; Xu, L.; Wang, C.; Wang, Y.; Li, Z.; Wang, Q.; Wang, D.N. Sub-micron silica diaphragm-based fiber-tip Fabry–Perot interferometer for pressure measurement. *Opt. Lett.* **2014**, *39*, 2827. [CrossRef]
91. Hou, M.; Zhu, F.; Wang, Y.; Liao, C.; Liu, S.; Lu, P. Antiresonant reflecting guidance mechanism in hollow-core fiber for gas pressure sensing. *Opt. Express* **2016**, *24*, 27890. [CrossRef]
92. Tang, J.; Yin, G.; Liao, C.; Liu, S.; Li, Z.; Zhong, X.; Wang, Q.; Zhao, J.; Yang, K.; Wang, Y. High-Sensitivity Gas Pressure Sensor Based on Fabry–Pérot Interferometer with a Side-Opened Channel in Hollow-Core Photonic Bandgap Fiber. *IEEE Photonics J.* **2015**, *7*, 1–7. [CrossRef]
93. Liang, M.; Fang, X.; Wu, G.; Xue, G.; Li, H. A fiber bragg grating pressure sensor with temperature compensation based on diaphragm-cantilever structure. *Optik* **2017**, *145*, 503–512. [CrossRef]
94. Song, X.; Hou, L.; Wei, X.; Su, H.; Li, C.; Li, Y.; Ran, L. High Sensitivity Fiber Gas Pressure Sensor with Two Separated Fabry–Pérot Interferometers Based on the Vernier Effect. *Photonics* **2022**, *9*, 31. [CrossRef]
95. Liu, T.; Zhang, W.; Wang, S.; Jiang, J.; Liu, K.; Wang, X.; Zhang, J. Temperature Insensitive and Integrated Differential Pressure Sensor for Liquid Level Sensing Based on an Optical Fiber Fabry–Perot Interferometer. *IEEE Photonics J.* **2018**, *10*, 1–8. [CrossRef]
96. Klimek, J.; Kisała, P.; Cięszczyk, S. Badanie Wpływu Parametrów Procesu Wytwarzania Periodycznych Struktur Światłowodowych na ich Charakterystyki Widmowe. Kraków. 2021. Available online: https://www.eaiib.agh.edu.pl/wp-content/uploads/2021/06/autoreferat-Klimek-Jacek.pdf (accessed on 17 September 2022).
97. Xu, M.G.; Reekie, L.; Chow, Y.T.; Dakin, J.P. Optical in-fibre grating high pressure sensor. *Electron. Lett.* **1993**, *29*, 398–399. [CrossRef]

98. Huang, J.; Zhou, Z.; Zhang, D.; Wei, Q. A Fiber Bragg Grating Pressure Sensor and Its Application to Pipeline Leakage Detection. *Adv. Mech. Eng.* **2013**, *5*, 1–6. [CrossRef]
99. Huang, J.; Zhou, Z.; Wen, X.; Zhang, D. A diaphragm-type fiber Bragg grating pressure sensor with temperature compensation. *Measurement* **2013**, *46*, 1041–1046. [CrossRef]
100. Pachava, V.R.; Kamineni, S.; Madhuvarasu, S.S.; Putha, K. A high sensitive FBG pressure sensor using thin metal diaphragm. *J. Opt.* **2014**, *43*, 117–121. [CrossRef]
101. Gu, Y.F.; Zhao, Y.; Lv, R.Q.; Yang, Y. A practical FBG sensor based on a thin-walled cylinder for hydraulic pressure measurement. *IEEE Photonics Technol. Lett.* **2016**, *28*, 2569–2572. [CrossRef]
102. Neeharika, V.; Pattnaik, P.K. Optical MEMS Pressure Sensors Incorporating Dual Waveguide Bragg Gratings on Diaphragms. *IEEE Sens. J.* **2016**, *16*, 681–687. [CrossRef]
103. Vorathin, E.; Hafizi, Z.M.; Aizzuddin, A.M.; Lim, K.S. A natural rubber diaphragm based transducer for simultaneous pressure and temperature measurement by using a single FBG. *Opt. Fiber Technol.* **2018**, *45*, 8–13. [CrossRef]
104. Leal-Junior, A.; Frizera, A.; Díaz, C.; Marques, C.; Ribeiro, M.; Pontes, M.J. Material features based compensation technique for the temperature effects in a polymer diaphragm-based FBG pressure sensor. *Opt. Express* **2018**, *26*, 20590–20602. [CrossRef]
105. Hegde, G.; Prasad, M.V.N.; Asokan, S. Temperature compensated diaphragm based Fiber Bragg Grating (FBG) sensor for high pressure measurement for space applications. *Microelectron. Eng.* **2021**, *248*, 111615. [CrossRef]
106. Wang, L.; Wang, Y.; Wang, J.; Li, F. A High Spatial Resolution FBG Sensor Array for Measuring Ocean Temperature and Depth. *Photonic Sens.* **2019**, *10*, 57–66. [CrossRef]
107. Jia, Z.; Fan, Q.; Feng, D.; Yu, D.; Zhao, X.; Yang, K. Design and investigation of the fiber Bragg grating pressure sensor based on square diaphragm and truss-beam structure. *Opt. Eng.* **2019**, *58*, 097109. [CrossRef]
108. Fan, Q.; Jia, Z.; Feng, D.; Yong, Z. Highly sensitive FBG pressure sensor based on square diaphragm. *Optik* **2021**, *225*, 165559. [CrossRef]
109. Liu, Z.; Zeng, L.; Xu, K.; Li, Z.; Chen, H.; Qiao, Z.; Qu, Y.; Liu, G.; Li, L. Design of a Fiber Bragg Grating Pressure Sensor Based on a Metal Diaphragm and Lever Structure. *Sensors* **2022**, *22*, 5096. [CrossRef]
110. Lu, S.; Chai, H.; Sahoo, A.; Phung, B.T. Condition Monitoring Based on Partial Discharge Diagnostics Using Machine Learning Methods: A Comprehensive State-of-the-Art Review. *IEEE Trans. Dielectr. Electr. Insul.* **2020**, *27*, 1861–1888. [CrossRef]
111. Raymond, W.J.K.; Illias, H.A.; Bakar, A.H.A.; Mokhlis, H. Partial discharge classifications: Review of recent progress. *Measurement* **2015**, *68*, 164–181. [CrossRef]
112. Sahoo, A.; Subramaniam, A.; Bhandari, S.; Panda, S.K. A review on condition monitoring of GIS. In Proceedings of the 2017 International Symposium on Electrical Insulating Materials (ISEIM), Toyohashi, Japan, 11–15 September 2017; pp. 543–546. [CrossRef]
113. Cheng, J.; Xu, Y.; Ding, D.; Liu, W. Investigation of sensitivity of the ultra-high frequency partial-discharge detection technology for micro-crack in epoxy insulator in GIS. *High Volt.* **2020**, *5*, 697–703. [CrossRef]
114. Gao, C.; Yu, L.; Xu, Y.; Wang, W.; Wang, S.; Wang, P. Partial Discharge Localization Inside Transformer Windings via Fiber-Optic Acoustic Sensor Array. *IEEE Trans. Power Deliv.* **2019**, *34*, 1251–1260. [CrossRef]
115. Ilkhechi, H.D.; Samimi, M.H. Applications of the Acoustic Method in Partial Discharge Measurement: A Review. *IEEE Trans. Dielectr. Electr. Insul.* **2021**, *28*, 42–51. [CrossRef]
116. Wang, Y.; Li, X.; Gao, Y.; Zhang, H.; Wang, D.; Jin, B. Partial Discharge Ultrasound Detection Using the Sagnac Interferometer System. *Sensors* **2018**, *18*, 1425. [CrossRef] [PubMed]
117. Nakano, Y.; Kozako, M.; Hikita, M.; Tanaka, T.; Kobayashi, M. Estimation method of degraded vacuum in vacuum interrupter based on partial discharge measurement. *IEEE Trans. Dielectr. Electr. Insul.* **2019**, *26*, 1520–1526. [CrossRef]
118. Chou, C.-J.; Chen, C.-H. Measurement and analysis of partial discharge of high and medium voltage power equipment. In Proceedings of the 2018 7th International Symposium on Next Generation Electronics (ISNE), Taipei, Taiwan, 7–9 May 2018; pp. 1–4. [CrossRef]
119. Su, H.-B.; Mo, W.-X.; Wang, Y.; Bi, F.; Ye, J.-B.; Gu, L. The Online Monitoring System of Vacuum Degree in High Voltage Vacuum Circuit Breakers Based on Electromagnetic Wave Method. In Proceedings of the 2020 IEEE International Conference on High Voltage Engineering and Application (ICHVE), Beijing, China, 6–10 September 2020; pp. 1–4. [CrossRef]
120. Kim, S.Y.; Hong, W.K.; Kim, M.H.; Jin, S.Y.; Kim, K.-H. A Comparative Study on the Partial Discharge Characteristics of Dry-air and SF6. In Proceedings of the 2022 6th International Conference on Electric Power Equipment—Switching Technology (ICEPE-ST), Seoul, Republic of Korea, 15–18 March 2022; pp. 267–270. [CrossRef]
121. Kim, N.-H.; Kim, D.-E.; Kim, S.-W.; Kil, G.-S. Comparative Analysis of Partial Discharge Characteristics of an Eco-Friendly Insulation Gas. In Proceedings of the 2022 6th International Conference on Electric Power Equipment—Switching Technology (ICEPE-ST), Seoul, Republic of Korea, 15–18 March 2022; pp. 294–297. [CrossRef]
122. Bang, S.; Lee, H.-W.; Lee, B.-W. Comparison of AC and DC Partial Discharge by Monitoring of Vacuum Degree in a Distribution Class Vacuum Interrupter. *IEEE Access* **2022**, *10*, 36254–36267. [CrossRef]
123. Wang, W.; Dong, J.X.; Yang, Y.; Miao, C.; Yue, B. On line measurement of vacuum degree based on continuous terahertz wave technology. In Proceedings of the 2020 5th Asia Conference on Power and Electrical Engineering (ACPEE), Chengdu, China, 4–7 June 2020; pp. 1736–1740. [CrossRef]

124. Caprara, A.; Cavallini, A.; Garagnani, L.; Guo, J. A Novel Approach for Continuous Monitoring of Partial Discharge Phenomena on Medium Voltage Equipments. In Proceedings of the 2018 IEEE Electrical Insulation Conference (EIC), San Antonio, TX, USA, 17–20 June 2018; pp. 495–498. [CrossRef]
125. Chung, I.-H.; Lin, Y.-H. Exploring the Impact of Parallel Architecture on Improving Adaptable Neuro-Fuzzy Inference Systems for Gas-Insulated Switch Defect Recognition. *Energies* **2022**, *15*, 3940. [CrossRef]

Disclaimer/Publisher's Note: The statements, opinions and data contained in all publications are solely those of the individual author(s) and contributor(s) and not of MDPI and/or the editor(s). MDPI and/or the editor(s) disclaim responsibility for any injury to people or property resulting from any ideas, methods, instructions or products referred to in the content.